Micromagnetic Realization of Energy-Based Models Using Stochastic Magnetic Tunnel Junctions

BingJin Chen^{a,1}, Yubo Hou², Chee Kwan Gan¹, Minggang Zeng^{a,2}

¹Institute of High Performance Computing (IHPC), Agency for Science, Technology and Research (A*STAR), 1 Fusionopolis Way, #16-16 Connexis, Singapore 138632, Republic of Singapore

²Institute for Infocomm Research (I2R), Agency for Science, Technology and Research (A*STAR),

1 Fusionopolis Way, #21-01 Connexis, Singapore 138632, Republic of Singapore

^aCorresponding authors: Chen BingJin@ihpc.a-star.edu.sg; zeng minggang@i2r.a-star.edu.sg

Abstract

Energy-based models (EBMs) can bridge physics, machine learning, and statistics. EBMs provide a unified and powerful platform to describe, learn, and optimize complex systems. In this paper, we propose a neuromorphic implementation of EBMs using a network of stochastic magnetic tunnel junctions (MTJs) that can perform energy minimization and solve optimization problems. Our implementation builds on the Object Oriented MicroMagnetic Framework (OOMMF). We derive the different energy terms and map them to the micromagnetic Landau-Lifshitz-Gilbert (LLG) equation. We then develop a C++ module for EBMs which integrates seamlessly with OOMMF. We demonstrate our implementation on a full set of logic gates using stochastic MTJs networks. Our method offers numerous advantages, including fast modeling of EBMs with spintronic devices and design insights for stochastic MTJ-based neuromorphic circuits.

•

I. Introduction

Modern digital computing that relies on accurate binary representations has raised several challenges in artificial intelligence (AI) applications such as speed limitation, data security, and power consumption [1,2]. Neuromorphic computing using stochastic MTJs [3–6] has recently emerged as a promising alternative computing scheme [7–12]. Stochastic MTJs utilize the stochastic nature of spin fluctuations in magnetic materials for computing and have shown great potential in areas such as cryptography [13], machine learning [10,14], and optimization [15]. One of the key advantages of stochastic MTJs is their ability to perform neuromorphic computation in a highly energy-efficient manner. Stochastic MTJs usually have low thermal energy barrier between their two distinct states and thus require low switching energy [16]. This allows significant reductions in power consumption and has the potential to enable the development of energy-efficient computing systems.

Several research groups have demonstrated the potential of stochastic MTJs for various computing tasks. For example, works have been carried to explore the potential of stochastic MTJs for cryptography [17]. Similarly, it has been demonstrated that MTJs can be used for combinatorial optimization tasks with orders of magnitude improvement in energy consumption compared to traditional approaches [18,19]. Other researchers have shown that stochastic MTJs can be used to perform deep neural network training with high accuracy and energy efficiency [20]. A network of interconnected stochastic MTJs can function as a powerful network of "p-bits", capable of performing a range of advanced neuromorphic computational operations [21–24]. These operations may include but are not limited to Boolean logic [16,24–26], combinatorial optimization [18,27], integer factorization [9], Bayesian inference [14,28], and data classification [29]. This technology represents a significant advancement in computing, as it provides a highly efficient means of processing complex data and solving intricate problems. Due to their lower hardware complexity and higher power efficiency compared to conventional CMOS circuits, stochastic MTJs networks may provide an efficient solution for building stochastic neural networks to perform complex computing tasks.

One can describe a system by its energy function. This allows us to study the system behaviours by minimizing the system energy or maximizing the system entropy. Therefore, energy-based models (EBMs) [30,31] provide a unified framework to bridge physics, machine

learning, and statistics. EBMs can describe object interaction in physics (e.g., Ising model), data distribution in machine learning (e.g., Boltzmann machine), and probability inference in statistics (e.g., Bayesian inference). Although EBMs offer a powerful design framework to exploit practical physical systems for probability programming, machine learning, and statistical applications, its implementation on analogy circuits is rare, partly due to the lack of suitable electronic devices and an efficient simulation platform. This article introduces an approach for implementing EBMs with stochastic MTJs in the micromagnetic framework. We demonstrate the potential of EBMs by leveraging a network of inter-connected stochastic MTJs to design a full set of logic gates. To do so, we map the energy function of the problem to the energy of the stochastic MTJs in the network, which can be implemented in micromagnetic simulation software such as OOMMF [32]. By performing dynamics micromagnetic simulations over time, the solution is obtained by the statistical magnetic distribution of the stochastic MTJ network.

II. Energy-based Models and micromagnetic formulation

The energy function for the states of a network of stochastic MTJs, $m=(m_1,m_2,...,m_N)$ can be written as

$$E(m) = -\sum_{i}^{N} b_{i} \cdot m_{i} - \frac{1}{2} \sum_{i}^{N} \sum_{j}^{N} m_{i} w_{ij} m_{j}.$$
 (1)

This energy function is the classical Ising model [33–39]. In the equation (1), N is the number of MTJs, b_i is a bias term acting on i-th stochastic MTJ (site i), w_{ij} is the coupling terms between site i and site j, and it is an anisotropy energy if i = j, m_i and m_j are unit magnetizations vectors at site i and site j, respectively. Both b_i and w_{ij} are learned parameters in the EBMs.

To minimize the energy in the equation (1), we apply OOMMF to do the micromagnetic simulations, in which numerical solutions that solve the Landau-Lifshitz-Gilbert (LLG) equation can predict the magnetic behavior of a system. The dynamics of magnetization m satisfies the LLG equations

$$\frac{dm}{dt} = -\gamma \mu_0 \left(m \times H_{eff} \right) + \alpha \left(m \times \frac{dm}{dt} \right), \tag{2}$$

where

$$H_{eff} = -\frac{1}{\mu_0 M_s} \frac{\partial U(m)}{\partial m}.$$
 (3)

Here U(m) is the total free energy of the magnetic system [40]. It is usually composed of anisotropy energy K_u , exchange energy K_{ex} , demagnetization energy K_d , Zeeman energy K_a , and thermal energy K_{th} . H_{eff} is the effective magnetic field associated with the total free energy, γ is the gyromagnetic ratio, α is the damping constant, μ_0 is the permeability constant, $m = M/M_s$ is the unit magnetization vector, with M the magnetization vector, and M_s is the saturation magnetization. All variables are in SI unit. For a magnetic system with uniaxial anisotropy field along z-axis, the effective fields from equation (3) can be written as

$$H_{eff} = \frac{K_u}{2\mu_0 M_s} m_z \vec{z} + H_{ex} + H_d + H_a + h_{th}, \tag{4}$$

where H_{ex} is the exchange coupling field, H_{d} is the demagnetization field, H_{a} is the applied field, and h_{th} is thermal field.

To implement the energy function expressed in equation (1) within micromagnetic framework, the energy function is rewritten as

$$E(m) = c_0(-\sum_{i=1}^{N} b_i \cdot m_i - \frac{1}{2} \sum_{i=1}^{N} \sum_{j=1}^{N} m_i w_{ij} m_j),$$
 (5)

where c_0 is a constant introduced to adjust the strength of the bias and the couplings. The effective fields associated with equation (5) are

$$H_{eff,i}^{E} = -\frac{1}{\mu_{0}M_{s}} \frac{\partial E(m)}{\partial m_{i}} = \frac{c_{0}}{\mu_{0}M_{s}} (b_{i} + \sum_{j}^{N} w_{ij} m_{j}), \tag{6}$$

where $H_{eff,i}^{E}$ denotes the effective field at site *i* associated with energy function expressed in equation (1). By combining the EBMs with micromagnetic simulations, we can make predictions about the magnetic behavior of systems according to the given energy functions.

In equation (6), the first term on the right-hand side corresponds to the Zeeman field, which arises from the interaction between the magnetic moment and an external magnetic field. The second term can be thought of as a distance-independent exchange coupling field that results from the interaction between the spin at site j and the spin at site i. In most micromagnetic software [32,41], only the exchange coupling field from the nearest neighbors is considered, but equation (6) suggests that this field may also have contributions from non-nearest neighbors. Therefore,

when implementing equation (6) in a micromagnetic simulation, it is important to consider all these coupling terms in addition to the nearest neighbor contributions typically considered.

III. Implementation of Energy-Based Models in OOMMF

Incorporating EBMs into the micromagnetic framework involves linking the energy function described in equation (1) with the total free energy of a network of stochastic MTJs. The stochastic nature of the MTJs enables the realization of the probabilistic aspect of the EBMs. By establishing this connection, we can gain insights into the underlying physics and solve optimization problems through simulating the behavior of a magnetic system under the influence of various stimuli. To do this, we wrote a C++ module to compute the effective fields based on the given energy function according to equation (6). Besides, we applied open source micromagnetic simulation software OOMMF [32] to get the statistical magnetization distribution of stochastic MTJ networks under a certain temperature. The bias term b_i and the coupling term w_{ij} are deemed as external inputs. For a network of stochastic MTJs with N spins, w_{ij} (i, j = 1, 2, ..., N; one spin for each MTJ) can take any value from the given energy function corresponding to a specific problem. This indicates that the micromagnetic realization of EBMs is universal for any energy function with a stochastic MTJ network.

The LLG equation for the dynamics of the magnetization m_i at site i is written as

$$\frac{dm_i}{dt} = -\gamma \mu_0 \left(m_i \times H_{eff,i} \right) + \alpha \left(m_i \times \frac{dm_i}{dt} \right), \tag{7}$$

where

$$H_{eff,i} = H_{eff,i}^E + H_K + h_{th}. (8)$$

Here H_K is the anisotropy field of the MTJ associated with the anisotropy energy K_u , h_{th} is the thermal fluctuation field [42], and $H_{eff,i}^E$ is the effective field associated with the given energy function, see equation (6). The three energy terms, i.e., anisotropy energy of an individual MTJ, total energy of the stochastic MTJ system and thermal energy, play crucial roles in this proposed modelling method.

MTJs are a type of spintronic device, as depicted in Figure 1(a). In an in-plane MTJ (*i*-MTJ), the magnetizations of both the reference layer (RL) and free layer (FL) lie in the plane. On the

other hand, in a perpendicular MTJ (p-MTJ), the magnetization is oriented perpendicular to the plane, as shown. Figure 1(b) illustrates how the anisotropy energy of the FL in an individual MTJ varies with its magnetization direction. The easy axis of magnetization, which corresponds to the two opposite directions with minimum anisotropy energy, determines the alignment of the magnetic moment. The difference between the maximum and minimum anisotropy energy, known as thermal barrier E_b , plays a crucial role in magnetization switching. In stochastic computing, E_b of stochastic MTJs is much lower than that in memory applications, resulting in low-energy computing [16,43]. Figure 1(c) depicts the total energy of a system as a function of various magnetization states of the MTJ network system, $m = (m_1, m_2, ..., m_N)$. The energy profile shows several local minimum states and a global minimum state. To avoid the system getting trapped in a local minimum, the random nature of the thermal field can be harnessed.

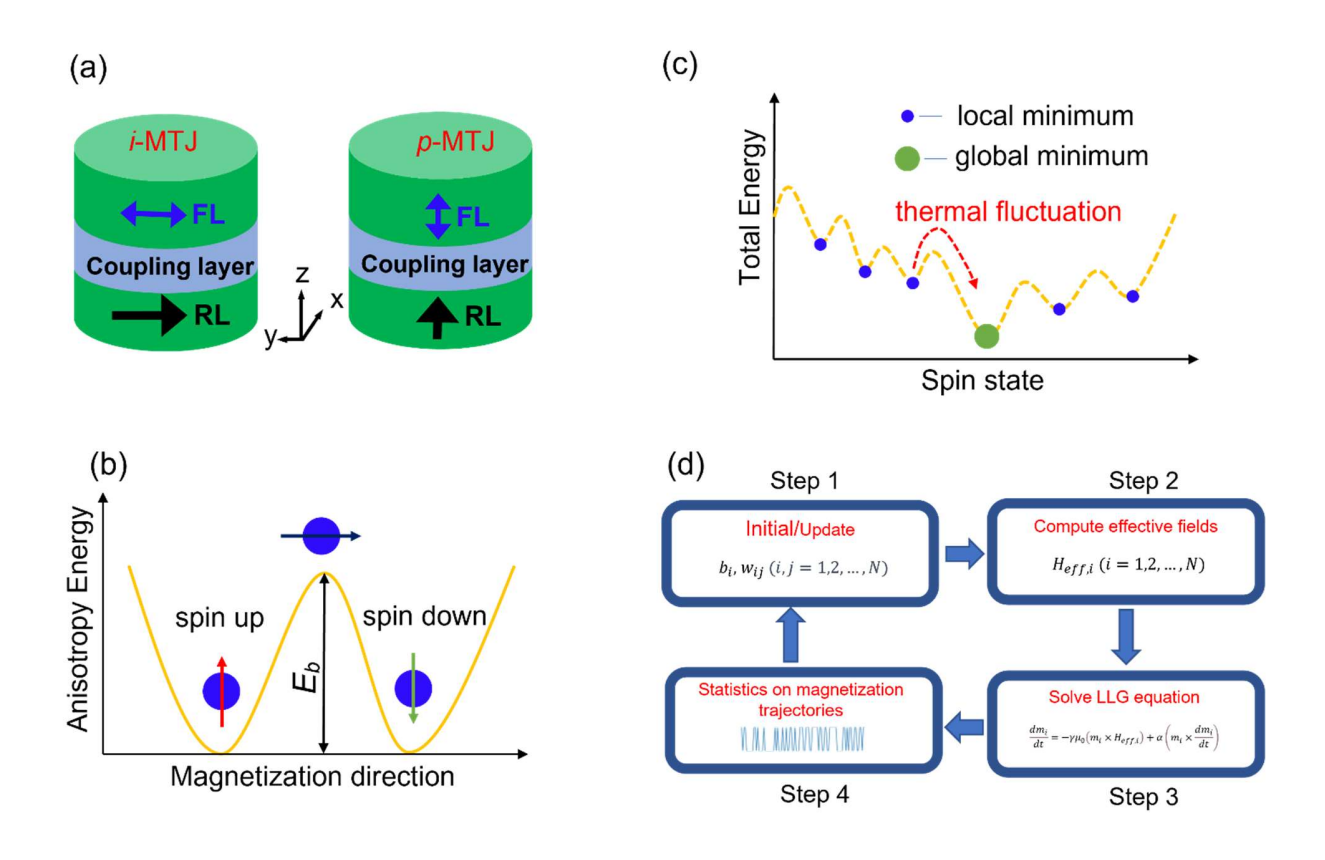


Figure 1. (a) Schematic of in-plane MTJ (*i*-MTJ) and perpendicular MTJ (p-MTJ). (b) Anisotropy energy of an individual stochastic MTJ as a function of magnetization directions. There are two opposite directions where the anisotropy energy is at its minimum and it is called the easy axis of magnetization in which a

magnetic moment is most likely to align. (c) Total energy of a system of the stochastic MTJs changes discretely with the states of the magnetizations $m = (m_1, m_2, ..., m_N)$. The energy profile has several local minimum states and a global minimum state. The thermal fluctuation prevents the system being stuck into a local minimum. (d) Main steps for implementing EBMs with a network of stochastic MTJs in micromagnetic simulations.

For a specific problem with given energy functions, the main steps for implementing it with a network of stochastic MTJs in micromagnetic simulation include: (i) Input initial bias b_i (i = 1,2,...,N) and the coupling w_{ij} (i,j = 1,2,...,N), (ii) compute effective field $H_{eff,i}$, (iii) solve the LLG equation, (iv) output and perform statistics on the dynamic trajectory of magnetization for each stochastic MTJ, and (v) update the bias b_i and w_{ij} coupling if needed, as shown in Figure 1(d).

IV. Stochastic MTJs for Logic Gates

In this section, we demonstrate how to integrate EBMs into the micromagnetic framework to design a full set of logic gates using stochastic MTJs. We focus on finding the truth tables for three basic but important logic operations, AND (\wedge), OR (\vee), and XOR (\oplus).

Using the Ising model, the Ising constraints for $m_3 = m_1 \wedge m_2$, $m_3 = m_1 \vee m_2$, and $m_3 = m_1 \oplus m_2$ can be written as [44–46]

$$H_{AND} = 3 - (m_1 + m_2 - 2m_3) - (-m_1 m_2 + 2m_1 m_3 + 2m_2 m_3). \tag{9}$$

$$H_{OR} = 3 - (-m_1 - m_2 + 2m_3) - (-m_1 m_2 + 2m_1 m_3 + 2m_2 m_3).$$
 (10)

$$H_{XOR} = 9 - (3m_4 - 3m_5 - 2m_3) - (-2m_1m_2 + 2m_1m_4 + 2m_1m_5 + 2m_2m_4) - (2m_2m_5 + 2m_3m_4 - 2m_3m_5 + m_4m_5),$$
(11)

or

$$H_{XOR} = 4 - (-m_1 - m_2 - m_3 - 2m_4) - (-m_1 m_2 - m_1 m_3 - 2m_1 m_4 - m_2 m_3 - 2m_2 m_4 - 2m_3 m_4).$$
(12)

In equations (9)-(12), $m_i(i=1,2,...,5) \in \{-1,+1\}$, is an Ising spin with index $i.m_1$ and m_2 are the input spins, m_3 is the output spin, while m_4 and m_5 are ancillary spins. Equations (9-12)

represent cost functions that are analogous to those used in the field of adiabatic quantum computing where networks of qubits are utilized to solve complex optimization problems [47,48]. Here we use the probabilistic bits from the stochastic MTJs. m_i represents the magnetization of the network of stochastic MTJs at site i. For a network of N stochastic MTJs, $m = (m_1, m_2, ..., m_N)$, total number of binary magnetization states is 2^N . For example, we need three stochastic MTJ (N = 3) for AND/OR problems [18,44,46], and four stochastic MTJs (N = 4 if use function in equation (12)) [45] or five stochastic MTJs (N = 5 if use function in equation (11)) [18] for XOR problem. To model the energy functions outlined in equations (9-12) in a micromagnetic framework, we utilize the approach that was introduced in the previous sections.

Table 1: Simulation parameters

Symbol	Parameter	Default value	Reference
$M_{\scriptscriptstyle S}$	Saturation magnetization	$1.115 \times 10^6 \text{A/m}$	Kanai <i>et al</i> .[49]
K_{in}	Intrinsic in-plane anisotropy	$5.575 \times 10^3 \text{J/m}^3$	Kanai <i>et al</i> .[49]
K_p	Effective perpendicular anisotropy	$-5.575 \times 10^5 \text{J/m}^3$	Kanai <i>et al</i> .[49]
α	Damping constant	0.02	Kanai <i>et al</i> .[49]
\boldsymbol{A}	Area of MTJ	$9 \times 10^{-16} \text{m}^2$	
t_F	MTJ Free layer thickness	1 nm	

Table 1 lists the material parameters used in the simulations for stochastic MTJs. Such stochastic MTJ has the relaxation time [49] less than 10 ns. Figure 2(a) shows the response of such a stochastic MTJ to an external spin current passing through it along the *x*-axis. The curve depicting the *x*-axis magnetization component showcases a sigmoidal shape in response to the spin current, where the average value increases rapidly at first, reaches a maximum, and then levels off as the spin current continues to increase. Figure 2(b) – Figure 2(f) visualizes the telegraph switching [50] nature of the such stochastic MTJ under the spin current excitations. Different spin currents induce different magnetization dynamics. Figure 2 indicates that the possibility of spin-up and spin-down states in a stochastic MTJ can be controlled by the spin current passing through it.

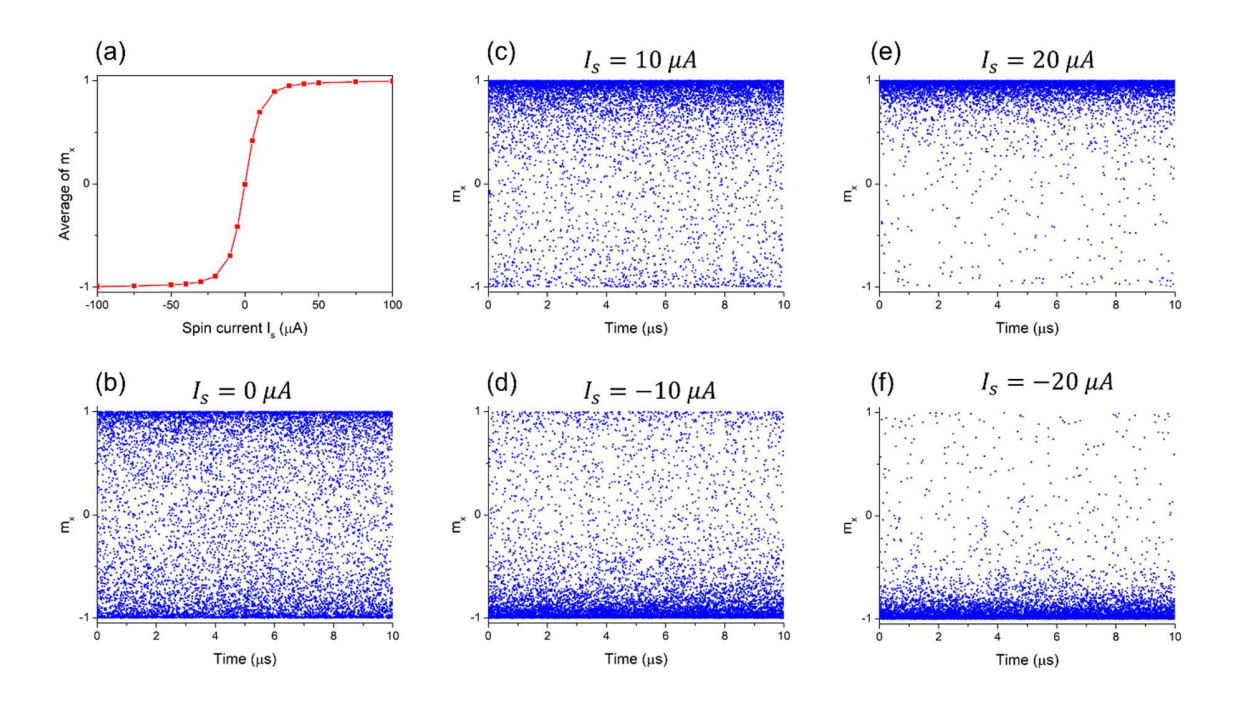


Figure 2. A stochastic MTJ responding to an external spin current. (a) The average magnetization component as a function of the spin current showing a sigmodal curve. (b)-(f) The x-axis magnetization component as function of simulation time for various spin currents showing different magnetization dynamics at different spin currents.

The preceding discussion lays the groundwork for the design of logic gates utilizing a stochastic MTJ network. In a network of stochastic MTJs, the bias and coupling terms for each individual MTJ dictate the possibility of its spin state according to the energy function. For AND/OR operation, we use a network of three stochastic MTJs and utilize the energy functions of equations (9) and (10). For XOR operation, we use a network of four stochastic MTJs, and utilize the energy function of equation (12). The input **b** and **W** used for micromagnetic simulations are shown in Figure 3 for (a) AND, and (b) XOR operations (for OR operation, **b** is replaced with its negative value, while **W** is the same as the AND operation).

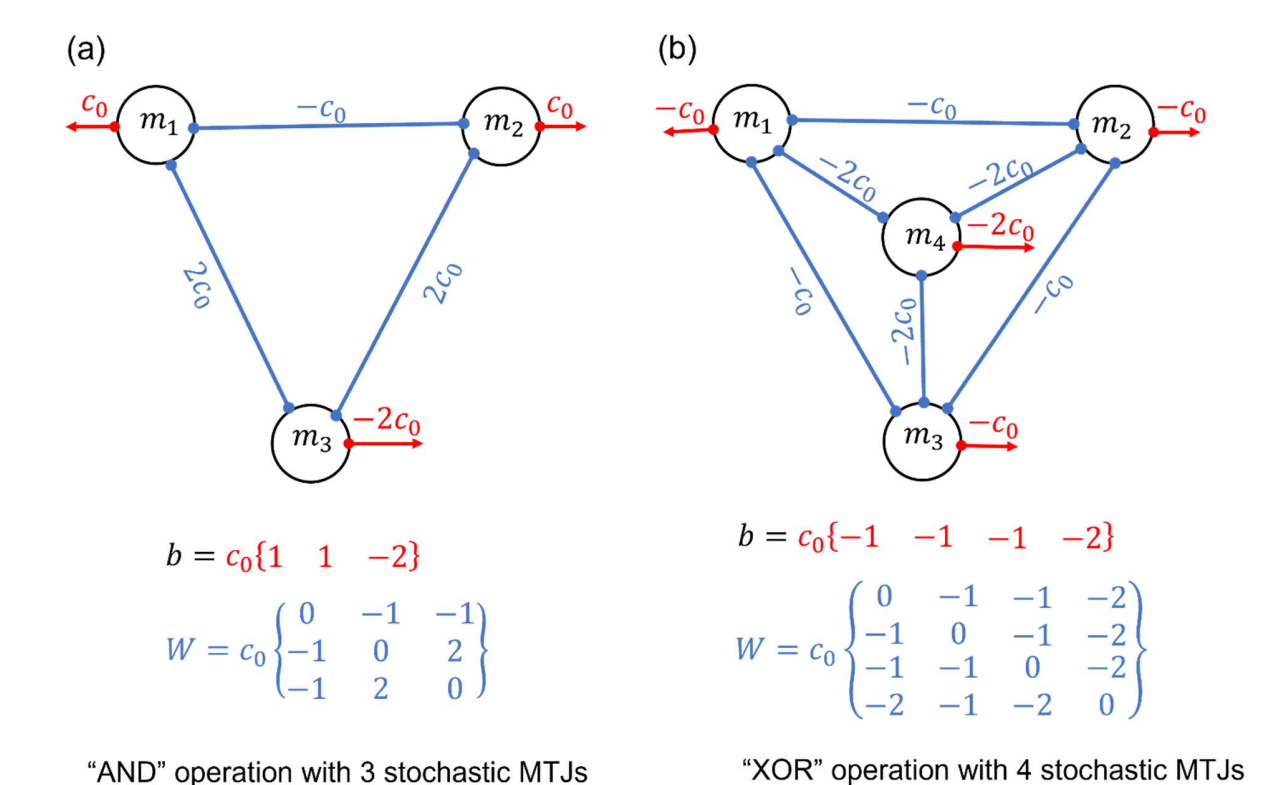


Figure 3. Energy functions and the inputs into micromagnetic simulations. (a) AND operation with three stochastic MTJs. (b) XOR operation with four stochastic MTJs. The MTJs are interconnected with **W** and biased with **b** according to the Ising constraints (energy functions).

The simulation results for the AND/OR operations using three stochastic MTJs are presented in Figure 4. In Figure 4(a), the x-component magnetizations for all three MTJs are plotted versus time for a period of 10 μ s. These values are digitized into binary (1, 0) and aggregated to determine their probability in +x and -x states respectively. Figure 4(b) visualizes the statistical results based on magnetization states in Figure 4(a) for the AND operation. The upper sub-figure shows the energy function at each time step according to the formula $h_{index} = m_1 + 2m_2 + 4m_3$, where $m_i(i = 1,2,3)$ are digitized into 0s if they are negative, and 1s if positive, as shown in Figure 4(d). Correspondingly, the lower sub-figure shows the histogram of energy function in 10000 timesteps. The truth table of AND operation can be identified from the histogram by choosing the top four states with the highest occurrences, i.e., the lowest energy, as shown in Figure 4 (e).

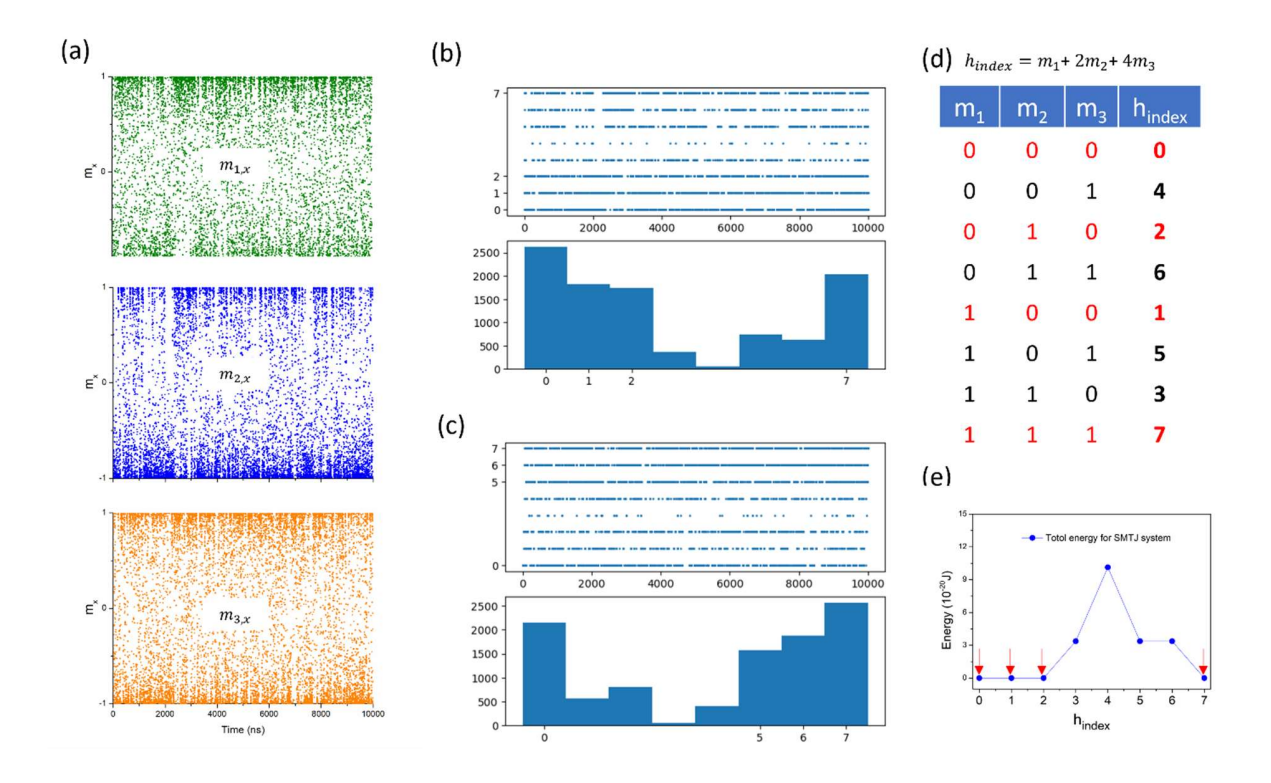


Figure 4. Micromagnetic simulation results for AND/OR operations with three stochastic MTJs. (a) The x-component magnetizations versus time for a period of 10 μ s. (b) Visualization of the statistic results based on magnetization states in (a) for AND operation. The index number (0-7) for the vertical axis of the upper sub-figure (and the horizontal axis of the lower sub-figure) is computed according to $h_{index} = m_1 + 2m_2 + 4m_3$, where $m_i(i=1,2,3)$ are digitized into 0s if they are negative, and 1s if positive. (c) Visualization of the statistic results for OR operation. (d) Eight magnetization states and their index values computed according to $h_{index} = m_1 + 2m_2 + 4m_3$. (e) The AND total energy for the stochastic MTJ system as a function of $h_{index} = m_1 + 2m_2 + 4m_3$, showing states 0, 1, 2, and 7 are in the lowest energy states, as indicated by red arrows.

A similar approach to the one used for the AND/OR operations is employed for the XOR operation using four stochastic MTJs. The magnetization states for all four MTJs are plotted in Figure 5(a) versus time for a period of 10 µs. These values are digitized and used to calculate the probability of occurrence for each possible state. Figure 5(b) presents the statistical results based on the digitized magnetization states from Figure 5(a). Like the AND operation, we can identify

the truth table of XOR by choosing the top four states with the highest occurrences, highlighted in red in Figure 5(c).

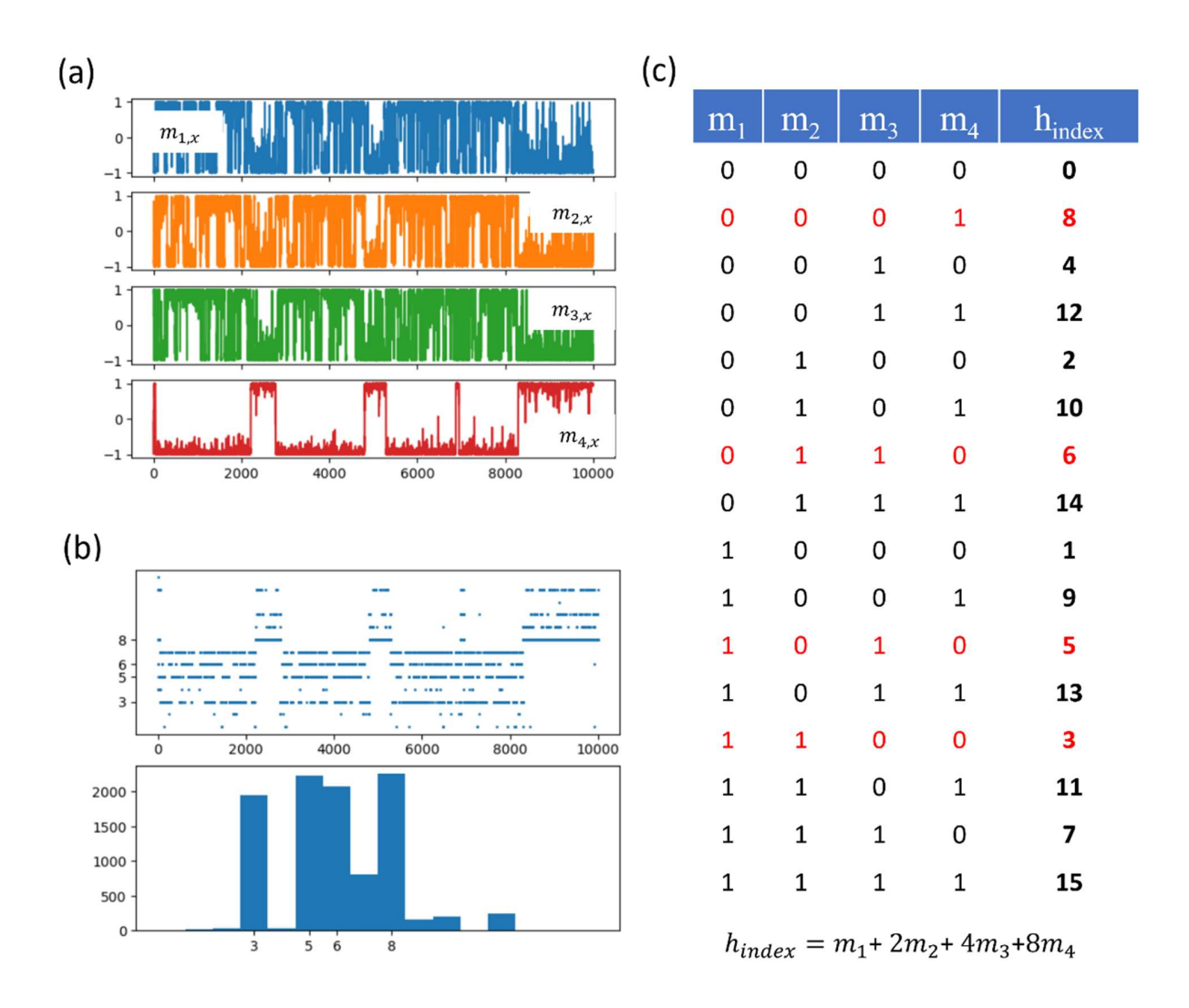


Figure 5. Micromagnetic simulation results for XOR operations with four stochastic MTJs. (a) The x-component magnetizations versus time for a period of 10 μ s. (b) Visualization of the statistic results based on magnetization states in (a). The index number (0-15) for the vertical axis of the upper sub-figure (and the horizontal axis of the lower sub-figure) is computed according to $h_{index} = m_1 + 2m_2 + 4m_3 + 8m_4$, where $m_i(i = 1,2,3,4)$ are digitized into 0s if they are negative, and 1s if positive. (c) Sixteen magnetization states and their index values computed according to $h_{index} = m_1 + 2m_2 + 4m_3 + 8m_4$.

Based on the observations in Figure 5(b), it can be inferred that while the four states with the highest occurrences (with h_{index} values of 3, 5, 6, and 8, respectively) correspond to the solution of the problem, there is another state (with an h_{index} value of 7) that also exhibits a relatively high occurrence. The observed behaviour can be attributed to an intrinsic property of the energy function presented in equation (12). Figure 6(a) illustrates the dependence the XOR total energy on $h_{index} = m_1 + 2m_2 + 4m_3 + 8m_4$ for the stochastic MTJ system. The plot includes the thermal barrier height $K_{in}V$ and a scale of the thermal energy k_BT for reference. The lowest zero energy states are identified with h_{index} values of 3, 5, 6, and 8, while the states with an h_{index} value of 7 belongs to the group of second lowest energy states. However, due to thermal fluctuation, the stochastic MTJ system may randomly transition from its lowest energy state to other states. In Figure 6(b), we illustrate the process of the stochastic MTJ system transitioning from the lowest energy states (3,5,6,8) to the second lowest energy states (e.g., 4,7) by flipping just one bit. This figure reveals that the stochastic MTJ system has a higher likelihood of transitioning from the lowest energy states to state 7 than to state 4 (or other second lowest states not shown). This observation explains why state 7 is relatively more frequently observed.

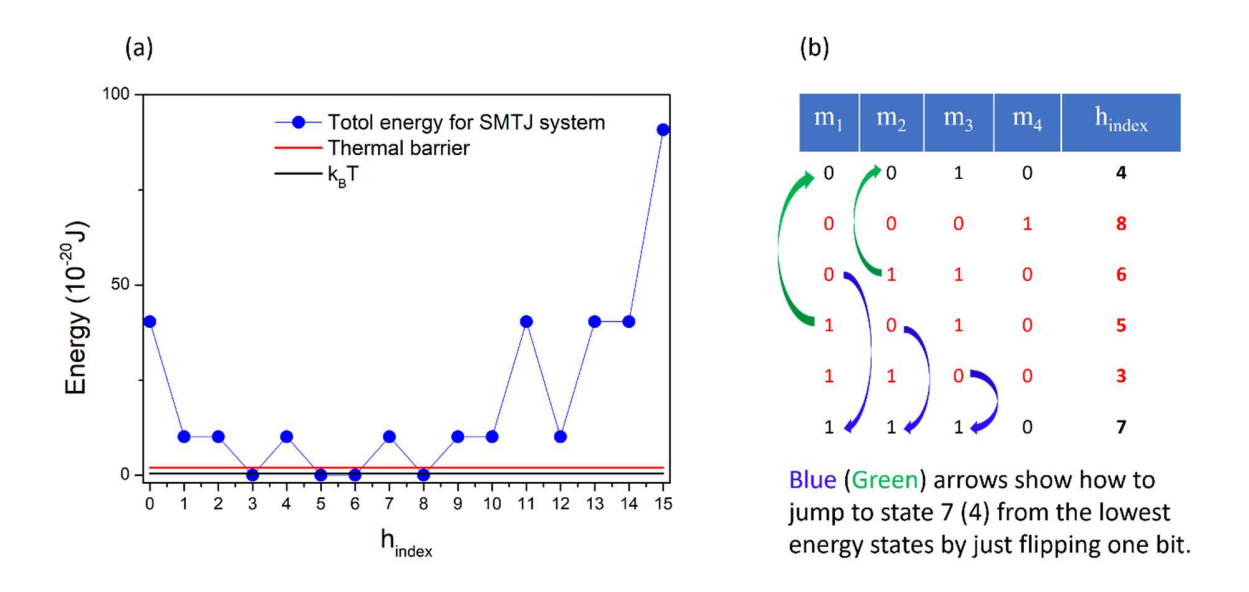


Figure 6. (a) Visualization of the XOR total energy for the stochastic MTJ system as a function of $h_{index} = m_1 + 2m_2 + 4m_3 + 8m_4$, showing states 3, 5, 6, and 8 are in the lowest energy states, while states 1, 2, 4, 7, 9, 10, and 12 are in the second lowest energy states. (b) A schematic representation of how the stochastic

MTJ system transitions from the lowest energy states to the second lowest energy states by flipping a single bit.

V. Conclusions

We have proposed an approach to implement energy-based models using the stochastic switching behaviors of magnetic tunnel junctions within the framework of OOMMF micromagnetic simulations. By interconnecting a network of stochastic MTJs with intrinsic stochastic switching behaviors, the probability of each possible system states, as defined by an energy function, can be correctly reflected by the statistical results of magnetization states, as demonstrated by the AND, OR, and XOR logic functions. This paves the way to solve the optimization problem, where the coefficient terms in the energy function can be optimized to find the lowest energy states of the stochastic MTJs network. The same strategy can be applied to energy-model based machine learning, where the network parameters, weights, and bias, can be trained for specific applications. We have demonstrated the efficient simulation of energy-based models using OOMMF. This helps to accelerate the development of neuromorphic computing with spintronic devices for future low-energy and fast deep learning applications.

Data Availability

The data that support the findings of this study are available from the corresponding authors upon request.

Declaration of Competing Interest

The authors declare that they have no known competing financial interests or personal relationships which could have appeared to influence the work reported in this paper.

Acknowledgment

This work is supported by Agency for Science, Technology and Research (A*STAR) under Career Development Fund (Project No. C210812054).

References

- [1] V. V. Zhirnov, R.K. Cavin, J.A. Hutchby, G.I. Bourianoff, Proc. IEEE 91 (2003) 1934–1939.
- [2] J.J. Yang, D.B. Strukov, D.R. Stewart, Nat. Nanotechnol. 8 (2013) 13–24.
- [3] K.Y. Camsari, M.M. Torunbalci, W.A. Borders, H. Ohno, S. Fukami, Phys. Rev. Appl. 15 (2021) 044049.
- [4] K. Kobayashi, W.A. Borders, S. Kanai, K. Hayakawa, H. Ohno, S. Fukami, Appl. Phys. Lett. 119 (2021) 132406.
- [5] K. Kobayashi, K. Hayakawa, J. Igarashi, W.A. Borders, S. Kanai, H. Ohno, S. Fukami, Phys. Rev. Appl. 18 (2022) 054085.
- [6] L. Yang, J.-P. Wang, in: 2017 IEEE Int. Electron Devices Meet., 2017, pp. IEDM17-801.
- [7] M.W. Daniels, A. Madhavan, P. Talatchian, A. Mizrahi, M.D. Stiles, Phys. Rev. Appl. 13 (2020) 034016.
- [8] Y. Wang, Y. Zhang, E.Y. Deng, J.O. Klein, L.A.B. Naviner, W.S. Zhao, Microelectron. Reliab. 54 (2014) 1774–1778.
- [9] W.A. Borders, A.Z. Pervaiz, S. Fukami, K.Y. Camsari, H. Ohno, S. Datta, Nature 573 (2019) 390–393.
- [10] J. Kaiser, W.A. Borders, K.Y. Camsari, S. Fukami, H. Ohno, S. Datta, Phys. Rev. Appl. 17 (2022) 014016.
- [11] J. Kaiser, S. Datta, Appl. Phys. Lett. 119 (2021) 150503.
- [12] A. Mizrahi, T. Hirtzlin, A. Fukushima, H. Kubota, S. Yuasa, J. Grollier, D. Querlioz, Nat. Commun. 9 (2018) 1–11.
- [13] B.R. Zink, Y. Lv, J.P. Wang, IEEE J. Explor. Solid-State Comput. Devices Circuits 8 (2022) 173–184.
- [14] S. Liu, T.P. Xiao, J. Kwon, B.J. Debusschere, S. Agarwal, J.A.C. Incorvia, C.H. Bennett, Front. Nanotechnol. 4 (2022) 1–16.
- [15] Y. Shim, A. Jaiswal, K. Roy, J. Appl. Phys. 121 (2017) 193902.
- [16] R. Faria, K.Y. Camsari, S. Datta, IEEE Magn. Lett. 8 (2017) 4105305.
- [17] C. Safranski, J. Kaiser, P. Trouilloud, P. Hashemi, G. Hu, J.Z. Sun, Nano Lett. 21 (2021) 2040–2045.

- [18] B. Sutton, K.Y. Camsari, B. Behin-Aein, S. Datta, Sci. Rep. 7 (2017) 1–9.
- [19] O. Hassan, A. Dissertation, Evaluation of Stochastic Magnetic Tunnel Junctions As Building Blocks for Probabilistic Computing, 2020.
- [20] T. Greenberg-Toledo, B. Perach, I. Hubara, D. Soudry, S. Kvatinsky, Semicond. Sci. Technol. 36 (2021) 114003.
- [21] N. Onizawa, D. Katagiri, W.J. Gross, T. Hanyu, Proc. 2014 IEEE/ACM Int. Symp. Nanoscale Archit. NANOARCH 2014 (2014) 59–64.
- [22] R. Zand, K.Y. Camsari, S. Datta, R.F. Demara, ACM J. Emerg. Technol. Comput. Syst. 15 (2019) 1–22.
- [23] F.X. Liang, P. Sahu, M.H. Wu, J.H. Wei, S.S. Sheu, T.H. Hou, 2020 Int. Symp. VLSI Technol. Syst. Appl. VLSI-TSA 2020 (2020) 151–152.
- [24] K.Y. Camsari, P. Debashis, V. Ostwal, A.Z. Pervaiz, T. Shen, Z. Chen, S. Datta, J. Appenzeller, Proc. IEEE 108 (2020) 1322–1337.
- [25] K.Y. Camsari, B.M. Sutton, S. Datta, Appl. Phys. Rev. 6 (2019) 011305.
- [26] K.Y. Camsari, R. Faria, B.M. Sutton, S. Datta, Phys. Rev. X 7 (2017) 1–19.
- [27] W. Chen, H. Tang, Y. Wang, X. Hu, Y. Lin, T. Min, Y. Xie, Micromachines 14 (2023) 258.
- [28] R. Faria, K.Y. Camsari, S. Datta, AIP Adv. 8 (2018) 045101.
- [29] A. Nisar, F.A. Khanday, B.K. Kaushik, Nanotechnology 31 (2020) 504001.
- [30] P. Huembeli, J.M. Arrazola, N. Killoran, M. Mohseni, P. Wittek, Quantum Mach. Intell. 4 (2022) 1–15.
- [31] M. Arbel, L. Zhou, A. Gretton, ArXiv:2003.05033 (2021).
- [32] M.J. Donahue, D.G. Porter, Interag. Rep. NISTIR 6376, Natl. Inst. Stand. Technol. MD (1999).
- [33] B.A. Cipra, Am. Math. Mon. 94 (1987) 937–957.
- [34] E. Vives, M.L. Rosinberg, G. Tarjus, Phys. Rev. B Condens. Matter Mater. Phys. 71 (2005) 134424.
- [35] U.B. Arnalds, J. Chico, H. Stopfel, V. Kapaklis, O. Bärenbold, M.A. Verschuuren, U. Wolff, V. Neu, A. Bergman, B. Hjörvarsson, New J. Phys. 18 (2016) 023008.
- [36] M.D. Leblanc, M.L. Plumer, J.P. Whitehead, J.I. Mercer, Phys. Rev. B Condens. Matter Mater. Phys. 82 (2010) 174435.
- [37] R. Gozdur, Algorithms 13 (2020) 134.
- [38] D.I. Albertsson, M. Zahedinejad, A. Houshang, R. Khymyn, J. Åkerman, A. Rusu, Appl. Phys. Lett. 118 (2021) 112404.

- [39] R. Behbahani, M.L. Plumer, I. Saika-Voivod, Phys. Rev. Appl. 18 (2022) 034034.
- [40] R. Bjørk, E.B. Poulsen, K.K. Nielsen, A.R. Insinga, J. Magn. Magn. Mater. 535 (2021) 168057.
- [41] A. Vansteenkiste, J. Leliaert, M. Dvornik, M. Helsen, F. Garcia-Sanchez, B. Van Waevenberge, AIP Adv. 4 (2014) 107133.
- [42] W.F. Brown, Phys. Rev. 130 (1963) 1677–1686.
- [43] A. Mondal, A. Srivastava, ACM J. Emerg. Technol. Comput. Syst. 16 (2019) 1–27.
- [44] J.D. Biamonte, Phys. Rev. A At. Mol. Opt. Phys. 77 (2008) 052331.
- [45] M. Gu, A. Perales, Phys. Rev. E Stat. Nonlinear, Soft Matter Phys. 86 (2012) 011116.
- [46] J.D. Whitfield, M. Faccin, J.D. Biamonte, Epl 99 (2012) 57004.
- [47] E.K. Grant, T.S. Humble, Oxford Res. Encycl. Phys. (2020) 1–23.
- [48] T. Albash, D.A. Lidar, Rev. Mod. Phys. 90 (2018) 15002.
- [49] S. Kanai, K. Hayakawa, H. Ohno, S. Fukami, Phys. Rev. B 103 (2021) 094423.
- [50] K. Hayakawa, S. Kanai, T. Funatsu, J. Igarashi, B. Jinnai, W.A. Borders, H. Ohno, S. Fukami, Phys. Rev. Lett. 126 (2021) 117202.